Investigating 4H-SiC Epilayer Thickness Variation in High-Resolution Ni/Y_2O_3/4H-SiC MOS Detectors

Ritwik Nag[1], Cihan Öner[2], Sandeep K. Chaudhuri[1], and Krishna C. Mandal[1]

[1]Department of Electrical Engineering, Molinaroli College of Engineering and Computing, University of South Carolina, Columbia, South Carolina, SC 29208, USA

[2]Department of Electrical and Electronics Engineering, Nevşehir Hacı Bektaş Veli University, Nevşehir 50100, Türkiye

Corresponding Author: Krishna C. Mandal (mandalk@cec.sc.edu)

Abstract: This study investigates the performance of Ni/Y_2O_3/4H-SiC metal–oxide–semiconductor (MOS) radiation detectors fabricated on 4H-SiC epilayers of 50, 150, and 250 µm thicknesses. The impact of epilayer thickness on electrical behavior, defect dynamics, and alpha particle response in Y_2O_3-gated 4H-SiC detectors is systematically examined. Leveraging the wide bandgap of 4H-SiC and the high dielectric constant and thermal stability of Y_2O_3, the devices are optimized for high-resolution radiation detection in harsh environments. A 40 nm Y_2O_3 dielectric layer, deposited via pulsed laser deposition, enables Schottky-like behavior and efficient charge transport. Device characterization included current–voltage and capacitance–voltage measurements to assess Schottky barrier properties, deep-level transient spectroscopy to analyze defect states, and alpha pulse height spectroscopy to evaluate detection response. The detector with a 250 µm epilayer exhibited the lowest leakage current and reduced concentrations and capture cross-sections of $Z_{1/2}$ and $EH_{6/7}$ traps—defects known to impair charge collection. However, despite these favorable electrical and defect characteristics, the 250 µm device showed a comparatively lower alpha detection response than thinner epilayer detectors. This behavior suggests an influence of the Y_2O_3/4H-SiC interface, particularly in thicker epilayers, where interfacial states or field distortions may hinder carrier transport. Overall, the findings provide new insights into optimizing thick epilayer MOS detector architectures and underscore the importance of interface engineering to advance robust, high-performance 4H-SiC-based radiation detectors for space, nuclear, and high-energy physics applications.

Keywords: 4H-silicon carbide (4H-SiC), Metal-oxide semiconductor (MOS), deep-level transient spectroscopy (DLTS), epitaxial layer, point defects, radiation detectors, Schottky barrier diode (SBD).

Relevance Summary:

- First systematic study of Ni/Y_2O_3/4H-SiC MOS detectors with 50–250 µm epilayers.
- Optimized 40 nm Y_2O_3 enables Schottky-like behavior with enhanced charge transport properties.
- Reveals unique Y_2O_3/4H-SiC interface effects on thick epilayer performance.
- Achieves record-low leakage current, high charge collection efficiency, and advances high-performance radiation detector design.

1. Introduction

The 4H polytype of silicon carbide (4H-SiC) offers several advantageous material properties that make it an excellent electronic material for radiation detection applications in harsh environment. Its wide bandgap (3.27 eV at 300K) contributes to a high breakdown electric field (3×10^6 V/cm), low leakage current, and low thermal noise and its exceptional thermal conductivity (490 W/m.K) allows for fast heat dissipation during high-temperature applications. The Si and C atoms in the 4H-SiC lattice have very high displacement thresholds making it far less susceptible to radiation induced displacement damages than conventional semiconductor devices in intense radiation environments. Epitaxially grown 4H-SiC thin films exhibit high crystallinity that enables to achieve high drift mobility of 1000 cm²/V-s [1] - [4]. Furthermore, the relatively low electron–hole pair (ehp) generation energy of 4H-SiC (7.28 eV) compared to ultra-wide bandgap semiconductors such as single crystalline diamond, Ga_2O_3, and GaN enables the generation of a higher number of charge carriers per incident particle, leading to superior energy resolution under comparable experimental and device conditions. In addition, unlike these materials—which often suffer from high fabrication costs, limited wafer availability, and lower growth yields—4H-SiC offers a mature, scalable, and cost-effective platform suitable for large-area radiation detector applications. [5]. The combination of the above properties makes 4H-SiC a superior harsh-environment electronic device material, specifically for radiation detectors in extreme environments such as nuclear reactor cores, space missions, and high-energy astrophysics.

Extensive research over the past few years has focused on reducing defect concentrations in 4H-SiC epitaxial layers to enhance charge collection efficiency and overall detector performance [6]. Studies have demonstrated that 4H-SiC alpha-particle detectors achieve energy resolutions comparable to those of silicon-based detectors [7] - [9]. Among different detector architectures, vertical Schottky barrier detectors (SBDs) are widely used due to their ability of high-resolution radiation detection [10]-[14].

Thick epitaxial layers are particularly useful for detecting penetrating radiation. The creation of a Schottky barrier on the surface of the epilayer facilitates the depletion of mobile charges within the epilayer. The depletion region constitutes the active detector volume, where charge pairs responsible for generating the detector signal are produced. While the present work focuses on alpha-particle measurements, thicker detectors are also of interest for detecting more penetrating radiation such as gamma rays and neutrons, where the increased active volume enhances interaction probability and overall detection efficiency. However, to fully deplete thick epitaxial layers require extremely high electric fields, which can lead to increased leakage currents—primarily due to surface conductivity—thereby degrading device performance. To mitigate this issue, dielectric layers are often employed to passivate semiconductor surfaces and to minimize surface leakage currents [15] - [17]. Additionally, incorporating a metal–oxide–semiconductor (MOS) structure helps reduce bulk leakage currents within the junction, further enhancing device performance and reliability [18].

While silicon dioxide (SiO_2) is the native oxide layer formed on 4H-SiC, its high interface trap density can result in increased leakage current, reduced channel mobility, and threshold voltage instability [6], [19] - [22]. To overcome these challenges, high-κ gate dielectrics such as HfO_2, Al_2O_3, TiO_2, CeO_2, La_2O_3, and Y_2O_3 [23] - [28], have been explored for deposition on 4H-SiC. The use of high-κ materials reduces the likelihood of premature dielectric breakdown, improves reliability, and lowers gate capacitance, thereby enhancing switching speed [18], [29].

Yttrium oxide (Y_2O_3) has emerged as a promising alternative to conventional high-κ dielectrics for wide bandgap semiconductor devices, particularly when integrated with 4H-SiC. Compared to the above mentioned high-κ materials, Y_2O_3 offers a unique combination of desirable properties, including a relatively high dielectric constant ($\kappa \approx 14 - 18$), exceptional thermal stability (up to ~2300 °C), and a wide bandgap of ~5.5 eV [30]. These characteristics are particularly advantageous for high-temperature applications, where dielectric reliability and interface integrity are critical. Additionally, Y_2O_3 exhibits good chemical compatibility with SiC and a favorable band alignment, which helps suppress leakage currents and minimize interface trap density [30]. In our earlier studies, we demonstrated that Ni/Y_2O_3/n-4H-SiC (NiYOSiC) vertical MOS radiation detectors exhibit significantly improved electrical and charge transport behavior compared to conventional Schottky barrier diodes, further highlighting the potential of Y_2O_3 as a superior dielectric material in SiC-based device platforms [31] - [33]. The results showed that a 40 nm Y_2O_3 layer on 20 µm-thick 4H-SiC epilayers yielded the best radiation detection performance, exhibiting high energy resolution and the highest reported charge collection efficiency (CCE) under self-biased operation.

In this study, we investigate radiation detectors comprising a fixed 40 nm-thick Y_2O_3 dielectric layer deposited on 4H-SiC epilayers of varying thicknesses, aiming to understand how the epilayer properties influence overall device performance. Although the Y_2O_3 layer remains constant, varying the epilayer thickness provides an opportunity to examine potential effects on electrical characteristics and radiation response. Differences in performance may be influenced by factors such as mechanical strain, thermal mismatch, or variations in interface quality, which can be indirectly affected by the underlying epilayer structure. The device interfaces were electrically characterized using current-voltage (I-V) and capacitance-voltage (C-V) measurements, and the detector response was evaluated through alpha-particle spectroscopy. Furthermore, deep level transient spectroscopy (DLTS) was employed to investigate point defects in the 4H-SiC epilayers, helping to discern whether the observed differences in device performance are attributable to intrinsic defects or the epilayer thickness.

2. Detector Fabrication

Three n-type 4H-SiC epitaxial layers with thicknesses of 50, 150, and 250 μm were used in this study. The samples are designated AS050, AS150, and AS250, respectively, based on their epilayer thicknesses. All epilayers, with an unintentional nitrogen doping concentration of approximately 10^{14} cm^{-3}, were homoepitaxially grown using a hot-wall chemical vapor deposition (CVD) method, following a consistent recipe [34]. Each epilayer was grown on the (0001) Si-face of a 350-μm-thick, heavily doped n-type 4H-SiC substrate (resistivity ≈ 0.028 Ω-cm), with a 4° off-cut toward the $\langle 11\bar{2}0 \rangle$ direction.

Square-shaped specimens (8 mm × 8 mm) were diced from the parent wafer for further processing. The samples were cleaned using the Radio Corporation of America (RCA) wafer processing protocol to remove organic and metallic contaminants [35]. Following the cleaning process, the wafers were immersed in a 10% diluted aqueous HF solution for 1 minute to etch away the native SiO_2 layer from the 4H-SiC surface before the oxide deposition.

The three 4H-SiC samples with different epilayer thicknesses were provided to the Nanostructured Materials for Energy Laboratory, located in the Department of Mechanical Engineering at the University of South Carolina, where epitaxial pulsed laser deposition (PLD) was performed to synthesize 40 nm-thick epitaxial Y_2O_3 thin films on the 4H-SiC epilayers. PLD offers several advantages for thin film growth, including precise control over film stoichiometry, accurate thickness tuning, and relatively high deposition rates [36]. For the growth of the Y_2O_3 oxide epilayers, a Coherent Inc. COMPex excimer laser operating at a wavelength of 248 nm was employed to ablate a Y_2O_3 ceramic disk target. The deposition was carried out using a laser fluence of 2 J/cm² and a repetition rate of 5 Hz, resulting in a growth rate of approximately 2.7 nm per minute. The 4H-SiC epilayer samples were affixed to the sample holder using silver epoxy on the bulk side of the samples and loaded into an NBM Design PLD chamber. During deposition, an oxygen partial pressure of 100 mTorr was maintained, and the substrate temperature was held at 700 °C to facilitate high-quality epitaxial growth.

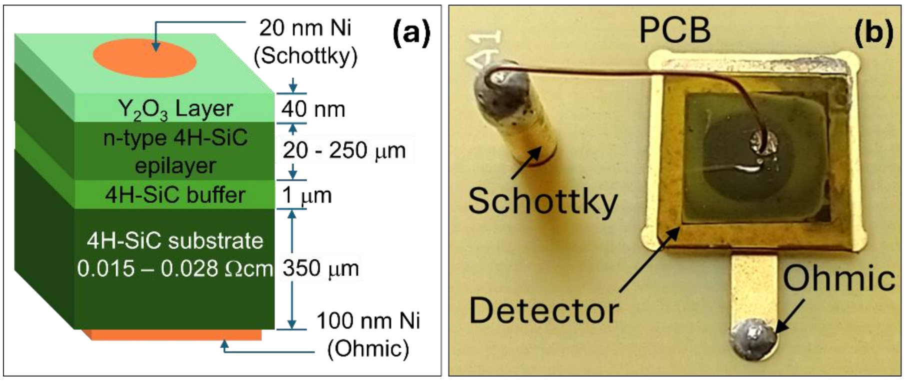

Fig. 1. (a) Schematic of a Ni/Y_2O_3/n-4H-SiC epitaxial MOS detector. (b) Photograph of an 8 mm x 8 mm detector mounted on a PCB. An unmounted bare detector was used for the C-DLTS measurements.

After the deposition, the residual silver paste was etched off from the bulk side of the 4H-SiC samples using nitric acid and thoroughly cleaned again. Metallization on the samples for electrical contacts were achieved by depositing 10 nm thick circular (diameter ~ 2.9 mm) nickel contacts on the top of Y_2O_3 thin films using a Quorum Q150T sputter coater. Additionally, 100 nm thick gold contacts with a much smaller diameter of 1 mm were sputtered on the top of the circular Ni contacts of each sample using a shadow mask to have stable contacts with the fine tipped probes for electrical measurements while leaving majority of the contact as semitransparent for radiation measurement purposes. Square shaped (6 mm × 6 mm) nickel contacts with a thickness of 100 nm were deposited on the bottom of the samples to form the Ohmic back contact. It may be noted that no post-deposition annealing was employed in this work. The high interface quality and stable Ohmic contacts were achieved through meticulous surface cleaning and preparation, highly polished epitaxial and bulk surfaces, and optimized doping profiles, which minimized interface defects and eliminated the need for additional thermal processing. The schematic of the detector structure has been shown in Fig. 1(a) and a photograph of the detector mounted on a printed circuit board (PCB) has been shown in Fig. 1(b).

3. Experimental Details

3.1. Electrical Characterization

I-V and high-frequency (1 MHz) C-V measurements were carried out at room temperature to characterize the interface/barrier properties. Room temperature I-V measurements were taken using a Keithley 237 source-measure unit with the detector mounted on a printed circuit board (PCB) and placed inside an electromagnetic interference shielded box. A Sula Technologies DDS-12 Deep Level Transient Spectrometer (DLTS) system equipped with a pulse generator unit, a capacitance meter unit, a pre-amplifier unit, and an interface to communicate with a PC based data acquisition and analysis software, was used for C-V measurements. In these measurements bare samples were mounted on the sample stage inside the liquid nitrogen cryostat of the DLTS set up and the measurements were carried out at room temperature.

3.2. Radiation Spectroscopy

Pulse-height spectroscopy measurements were carried out to evaluate the radiation detection response of the detectors. A 0.9 µCi ^{241}Am radioisotope emitting alpha particles α_1, α_2, and α_3 with energies 5486 (85%), 5443 (14%), and 5381 (1%) keV, respectively, was used as a test source. The detector, mounted on a PCB and the alpha-source, was placed inside an electromagnetically shielded box continually evacuated using a vacuum pump to minimize the scattering of alpha particles with the air molecules. The detector signal was fed to a Cremat CR110 charge-sensitive preamplifier. The output of the preamplifier was fed to a standard benchtop alpha spectrometer comprising an Ortec 671 spectroscopy amplifier and a Canberra Multiport II multi-channel analyzer (MCA) module controlled by Genie 2000 data acquisition software. An absolute calibration method was used to convert the channel numbers in the MCA to energy (keV) units, as reported in our previous publication [37].

3.3. Deep-level Transient Spectroscopy (DLTS)

The DLTS measurements were conducted using a Sula Technologies DDS-12 deep-level transient spectrometer [18, 33]. Bare samples were placed onto a temperature-controlled copper stage housed within a VPF-800 liquid nitrogen-cooled cryostat. The temperature of the copper stage was regulated using a Lakeshore LS335 temperature controller. The detector was connected to a bias supply and a pulse generator module. A steady-state reverse bias of -12 V was applied. The traps under investigation were electrically filled by pulsing the devices to 0 V from the steady state-state reverse bias with a pulse duration ranging from 5 to 1000 ms depending on the selected rate window. A pulse width of 2 ms was used to ensure saturated trap filling. Once the filling pulse ended, the trapped charges were released, and the capacitance gradually returned to its initial value forming the capacitance transients. To obtain the DLTS spectra temperature scans typically in the range 80 – 800 K were carried out with an increment of 1K. The capacitance transients were analyzed at each temperature. During the temperature scans, a peak in the DLTS spectrum was observed when the emission rate of a specific trap matched the set rate window. The rate windows were configured using a digital boxcar averaging technique. A dedicated data acquisition and analysis program processed the pulse signals to generate DLTS spectra. Key defect characteristics, such as trap concentration, capture cross-section, and energy level, were determined through analysis of the DLTS spectrum and Arrhenius plots.

4. Results

4.1. Electrical Characterization

Figure 2 presents the dark current as a function of gate bias (I–V characteristics) for both bias polarities for all three devices, measured at room temperature. The strong asymmetry in current density with respect to bias polarity highlights the pronounced rectifying behavior of the MOS junctions. As summarized in Table I, the current density at a bias of –500 V ranges between 1×10^{-10} and 7×10^{-10} A/cm². A slight decrease in leakage current density is observed with increasing epilayer thickness from AS050 to AS150 and AS250. The lower leakage current—by approximately a factor of six for the 150 µm and 250 µm detectors—may be attributed to the wider depletion region available at higher bias voltages. Overall, the reverse leakage currents remain low and comparable among all detectors. Since the I-V characteristics resembled Schottky behavior, a thermionic model applicable to Schottky barrier diodes as given below in (1) has been used to obtain the interfacial properties such as the ideality factor (n) and Schottky barrier height (Φ_B) [38]. Also, the positive and negative polarity bias at the top circular Ni contact measured with respect to the bulk side square Ni contact, will be referred to as the forward and reverse bias, respectively, henceforth.

$$J = A^{*}T^{2}\left(e^{-\frac{q}{k_B T n}\Phi_B}\right)\left(e^{\frac{q}{k_B T n}V} - 1\right) \quad (1)$$

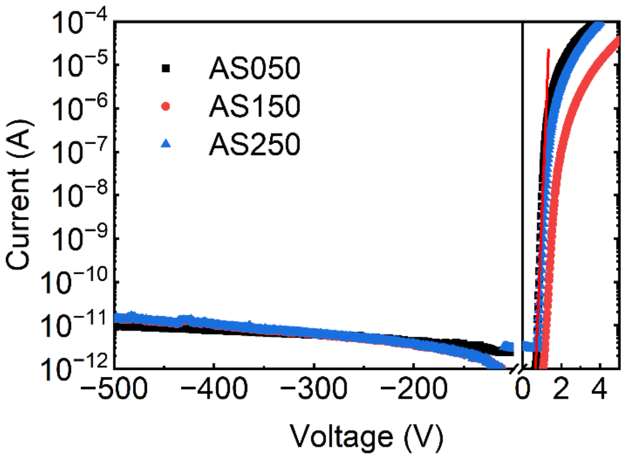

Fig 2. Variation of junction current as a function of forward (positive) and reverse (negative) bias (I–V characteristics) for the AS050, AS150, and AS250 MOS detectors. The solid red line represents a linear fit to the AS050 I–V data based on the thermionic emission model described by Equation (1).

Where A^* is the Richardson constant for 4H-SiC (146 A/K^2/cm^2), T is the absolute temperature of the diode, q is the elementary charge, and k_B is the Boltzmann's constant. The diode parameters extracted using (1) are listed in Table I. As observed in our previous study, the presence of the interfacial oxide layer in MOS devices influences the bulk current by increasing the Schottky barrier height, reducing tunneling probability, and mitigating surface leakage through passivation effects [18]. In general, a diode ideality factor close to unity suggests a homogeneous barrier height distribution across the contact area but as seen in Table I, the higher ideality factors observed in the three devices indicate inhomogeneous barrier heights, likely due to local structural defects [39] - [41]. The deviation of the ideality factor from unity arises from spatial variations in the Schottky barrier height across the device surface, leading to localized current flow through regions of lower barrier height. Such effects, rather than uniform interface states or recombination mechanisms, can result in ideality factors greater than unity—and in some cases exceeding two—depending on the degree of barrier non-uniformity. These regions contributed to lower barrier height and hence to increased leakage.

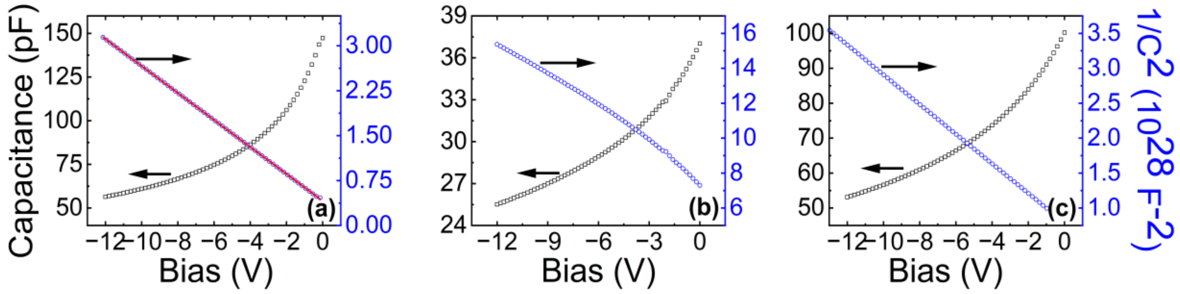

Fig 3. Variation of junction capacitance as a function of bias (in black squares, plotted on the left y-axis) and the corresponding Mott-Schottky plots (in blue circles, plotted on the right-y axis) for AS050 (a) AS150 (b) and AS250 (c) MOS detectors.

Figure 3(a)-(c) presents the Mott–Schottky (1/C^2 vs V) plots obtained from the capacitance–voltage (C-V) measurements. Based on a parallel-plate capacitance model, a linear fit to the Mott–Schottky data allows extraction of the effective doping concentration N_{eff} and built-in potential V_{bi} using the equation [38]:

$$\frac{A^2}{C^2} = \frac{2}{(N_{eff}q\varepsilon_0\varepsilon_{4H-SiC})}\left(V_{bi} - V - \frac{k_B T}{q}\right) \quad (2)$$

Here, A denotes the contact area, ε_0 is the electrical permittivity of vacuum and ε_{4H-SiC} = 9.7 is the dielectric constant of 4H-SiC. The variation in N_{eff} ranges from (0.5 – 2) × 10^{14} cm^{-3}, aligns with the spatial doping concentration variations observed across the 10 cm-diameter parent wafers. Among all detectors, AS250 exhibited the lowest N_{eff} which is advantageous for achieving a wider depletion region at a given bias. The lower N_{eff} observed in AS250 is specific to the present sample and results from slight unintentional doping non-uniformities across the 4-inch parent wafer.

4.2. Radiation Detection

Figures 4(a) & (c) depict the pulse height spectra recorded for the three MOS detectors at their respective optimized operating voltages and a shaping time of 2 μs. In both the detectors all the primary alpha peaks viz. α_1, α_2, and α_3 were observed to be well-resolved depicting the high energy-resolution of the detectors. The peaks were fitted using a multiple Gaussian peak fitting program to determine crucial peak parameters such as the full width at half maximum ($fwhm$) and the peak centroid (E_p). The percentage energy resolution of the detectors for the 5486-keV (α_1) peak listed in Table I has been calculated as $(fwhm/E_p) \times 100$. Percentage energy

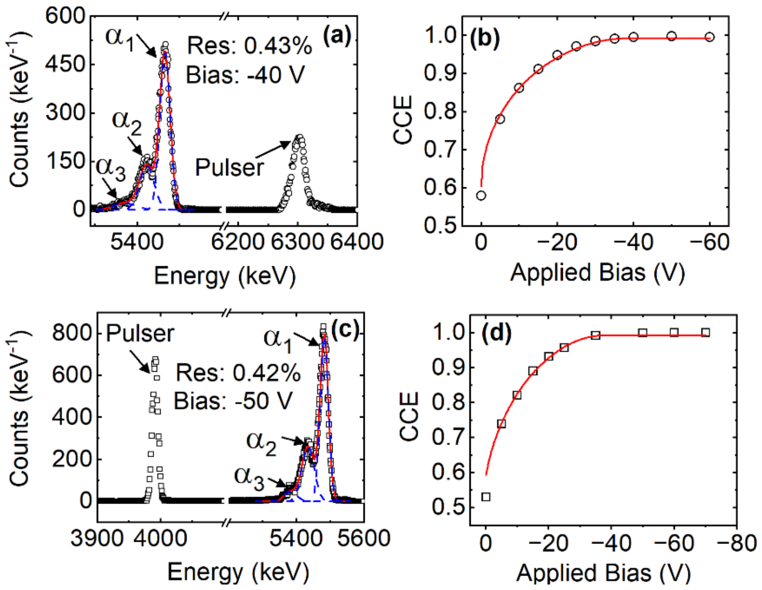

Fig. 4. Pulse height spectra with three distinct α-peaks recorded with the AS050 (a) and AS150 (c) detectors exposed to the ^{241}Am alpha emitting source under optimised settings (Shaping time = 2 μs). The dotted lines show the Gaussian fitting of the individual peaks while the solid line shows the cumulative peak fitting. The variation of the CCE measured for the 5486-keV alpha peaks as a function of the reverse bias for the AS050 (b) and AS150 (d) detectors. The solid lines are the fits following a drift-diffusion model given by (3).

resolution of ≈0.4% for the 5486-keV alpha peak, as observed for the AS050 and AS150, is indeed among the reported high energy resolution detectors. The AS250 detector showed a relatively lower energy resolution (higher $fwhm$) and will be discussed in detail in the following sections. The optimum bias voltages, corresponding depletion widths, and percentage energy resolutions are listed in Table 1 for ease of comparison. It may be noted that the detectors are only partially depleted at these voltages. Nevertheless, this level of depletion is sufficient for the present alpha-particle measurements, as their penetration depth is approximately 18 μm. With suitable high-voltage adjustments and careful biasing measures, the detectors can be fully depleted for the detection of more penetrating radiation such as gamma rays.

Figure 4(b) & (d) illustrates the variation in charge collection efficiency (CCE) as a function of negative gate bias for the AS050 and AS150 detectors. The CCE corresponding to the α_1 peak has been calculated as the ratio $E_p/5486$. The CCE for all detectors was modeled using a drift-diffusion framework, as expressed in equation (3), which describes how the theoretical CCE (η_{theory}) varies with applied bias in Schottky-type junctions [42]:

$$\eta_{theory} = \frac{1}{E_i}\left[\int_0^d \left(\frac{dE_i}{dx}\right) + \int_d^{x_r}\left[\left(\frac{dE_i}{dx}\right) dx \times e^{\left\{-\frac{(x-d)}{L_d}\right\}}\right] dx\right]$$
$$= \eta_{drift} + \eta_{diffusion} \quad (3)$$

In the above equation, d is the depletion width at a set bias, x_r is the penetration depth of the incident alpha particles in 4H-SiC, x is the distance measured from the metal/Y_2O_3 interface, dE/dx is the electronic stopping power of the alpha particles calculated using SRIM-2008—a simulation tool that models ion interactions with matter [43].The first term, η_{drift}, accounts for charge carriers generated within the depletion region that contribute to CCE through drift under an applied electric field. The second term, $\eta_{diffusion}$, represents this contribution due to diffusion of charge carriers produced beyond the depletion region.

To determine the hole diffusion length (L_d), experimental CCE values (η_{exp}) were fitted to (3). Table 1 lists the extracted L_d values, revealing that detectors AS150 showed higher hole diffusion length. A larger L_d suggests reduced hole trapping, implying a lower density of hole-trapping defects in these devices, which was slightly higher than AS050.

Table I further summarizes the percentage energy resolutions under optimal bias condition. For all detectors except AS250, the relative peak intensities aligned well with the expected intensity ratio of α_1, α_2, and α_3. However, in the case of AS250, the two alpha components, α_2 and α_3, could not be deconvoluted due to the poorer resolution of the detector compared to the other two. Also, at lower bias voltages no discernable peaks could be obtained which limited our ability to obtain readings at low bias voltages, and consequently, fitting to the drift-diffusion model could not be performed. However, both detectors, AS050 and AS150 successfully generated distinct alpha peaks even in self-biased mode (0 V applied bias). AS050 delivered the best energy resolution, achieving the lowest FWHM at its optimal bias.

Table 1. Device properties obtained from electrical measurements.

Sample ID	Ideality Factor	Barrier Height (eV)	Effective Donor Conc. (cm^{-3})	Leakage Current Density @ -500 V (A/cm^2)	Operating Bias (V)	Depletion Width at Operating Bias (µm)	5486 keV Resolution (%)	Minority Carrier Diffusion Length (µm)
AS050	1.34	1.57	1.46×10^{14}	6.78×10^{-10}	-40	17.1	0.43	28
AS150	1.67	1.50	1.55×10^{14}	1.16×10^{-10}	-50	18.5	0.42	32
AS250	1.97	1.42	5.22×10^{13}	1.2×10^{-10}	-60	34.9	0.81	-

4.3. Deep-Level Transient Spectroscopy (DLTS)

Figure 5(a)-(f) presents the DLTS spectra for a set of four rate windows obtained from the three different detectors. Figures 6(a) – (c) shows the Arrhenius plots of all the peaks for the three detectors. Each peak in the DLTS spectrum corresponds to an individual trap center or a combination of unresolved trap states. The peak positions (T_m) on the temperature axis of a DLTS spectrum align with the emission rate (e_n) set by the boxcar rate window τ_m, where $\tau_m = 1/e_n$.

The theoretical relationship governing the variation of e_n/T_m^2 with temperature can be expressed as [44]:

$$e_n = \left(\frac{\sigma_n \langle v_{\rm th}\rangle N_C}{g1}\right) \exp\left(\frac{-\Delta E}{kT}\right) \tag{4}$$

where σ_n is the capture cross section, $\langle v_{\rm th}\rangle$ is the mean electron thermal velocity, which varies as $T^{1/2}$; N_C is the effective density of states in the conduction band which varies as $T^{3/2}$; $g1$ is the degeneracy of the trap level, which is assumed to be unity; and ΔE is the activation energy defined as the location of the trap energy level measured with respect to the conduction band minimum. Since the temperature-dependent factors in $\langle v_{\rm th}\rangle$ and N_C combine to yield a T^2 dependence, a linear fit to the Arrhenius plot [$\ln(e_n/T^2)$ vs. $1000/T$] provides an estimate of both the activation energy and the capture cross-section for each defect state. The concentration of deep-level traps N_t was determined using (5) below [44]. All the above defect parameters have been calculated and listed in Table II for each identifiable peak observed in each of the detectors.

$$N_t = 2\left(\frac{\Delta C}{C_0}\right)(N_{eff}) \tag{5}$$

All the three detectors showed three distinct peaks P1, P2, and P3 located respectively around 0.14, 0.18, and 0.67 eV below the conduction band edge E_C. The activation energies have been given in Table II. These peaks are commonly noticed in our 4H-SiC epilayers. The first two peaks correspond to the substitutional titanium impurity centers Ti(h) and Ti(c) that occupies the hexagonal and cubic Si sites, respectively. These trap centers are considered as shallow levels and do not participate in trapping that may substantially affect the device performance.

The peak P3 is the $Z_{1/2}$ center that is attributed to carbon vacancies or vacancy-related complexes. They are commonly referred to as “lifetime-killer” defects due to their strong impact on carrier recombination and charge collection efficiency. The $Z_{1/2}$ center is one of the most critical trap centers affecting the performance of our radiation detectors [45] - [47].

Unlike the well-resolved and symmetric peaks discussed earlier, the apparent asymmetry observed in the fourth peak (P4) clearly indicates the presence of unresolved peaks associated with multiple trapping centers having closely spaced activation energies. Due to this overlap, the individual components could not be deconvoluted, and only the dominant peak, designated as P4, was analyzed. The activation energy of P4 was determined to be 1.56, 1.55, and 1.42 eV from the conduction band minimum for the detectors AS050, AS150, and AS250, respectively. These levels are generally attributed to carbon vacancies or carbon–silicon divacancies, commonly referred to as $EH_{6/7}$ centers [48] - [51]. $EH_{6/7}$ centers are known electron traps and have been observed to impact device performance fabricated in our laboratory.

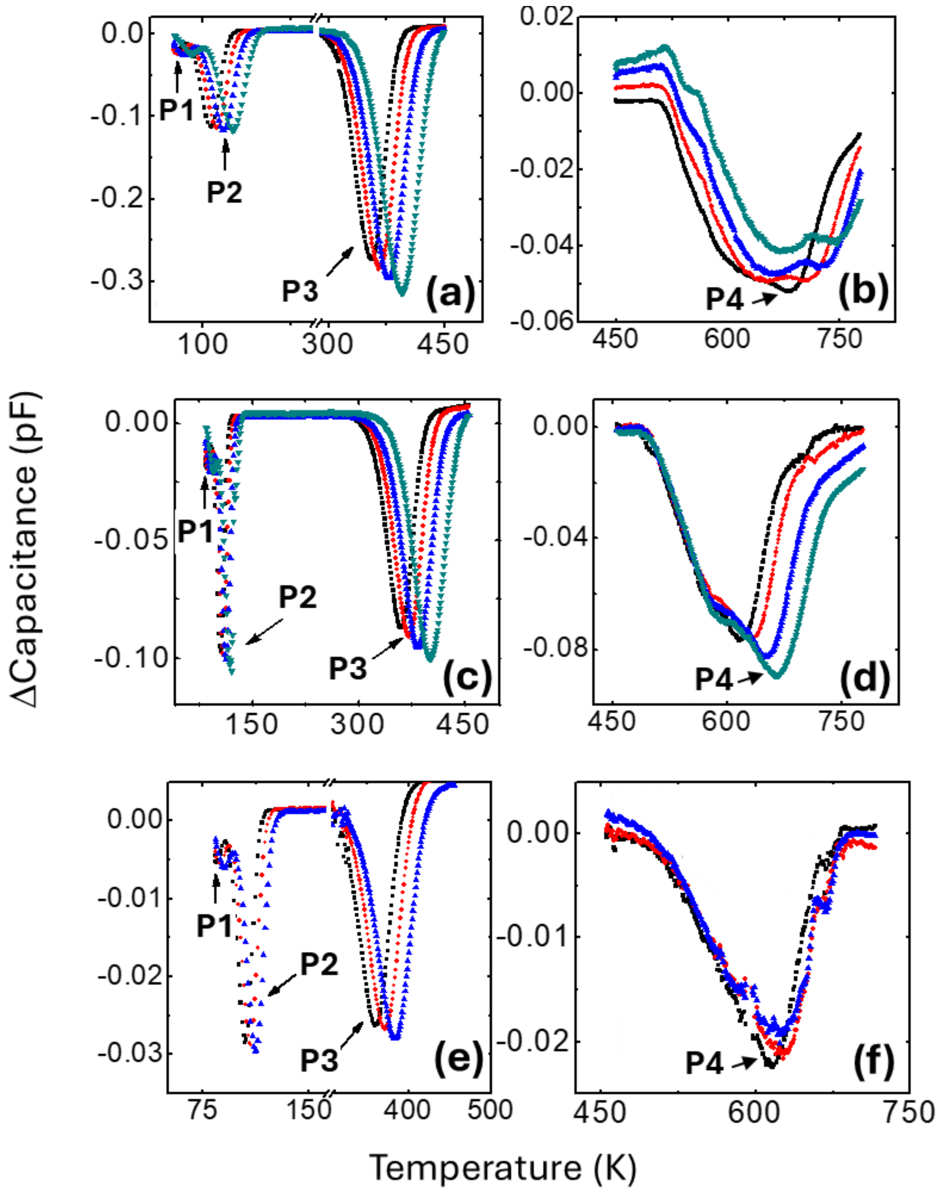

Fig 5. DLTS spectra obtained for the AS050 (a), AS150 (b) and AS250 (c) MOS detectors in the temperature range 80 – 800 K. A set of four rate windows out of twelve has been shown in the figure.

Point defects or trapping centers such as $Z_{1/2}$ and $EH_{6/7}$ in 4H-SiC epilayers can capture charge carriers generated by incident radiation, reducing the number of carriers contributing to the output signal. This carrier trapping leads to incomplete charge collection, thereby lowering charge collection efficiency and broadening the energy spectrum, ultimately degrading the detector's energy resolution. Defects with higher concentrations or larger capture cross-sections exert a more pronounced impact by increasing the likelihood of trapping events during carrier transit. Interestingly, as shown in Table II, the trap concentrations and capture cross-sections of the dominant $Z_{1/2}$ and $EH_{6/7}$ centers in the AS250 detector are significantly lower than those in AS050 and AS150. Yet, AS250 exhibited inferior radiation detection performance compared to the thinner epilayer detectors. Notably, Schottky barrier detectors (without the Y_2O_3 layer) fabricated on 250 µm-thick 4H-SiC sister samples with similar defect concentrations and capture cross-sections demonstrated performance comparable to AS050 and AS150 [13], [34], [52]. These findings suggest that the degraded performance of AS250 is not primarily caused by electron trapping at deep-level defects but may instead originate from variations in the physical or electrical characteristics of the Y_2O_3/4H-SiC interface. In particular, interface states resulting from differences in surface quality, residual stress from the SiC growth process, or microstructural non-uniformities prior to oxide deposition could contribute to the observed behavior. However, this observation may also be specific to the present sample set and may not reflect a general trend associated with epilayer thickness. Other mechanisms, such as bulk defects or charge-trapping effects, could also play a role. Further investigations, including detailed electrical characterization of interfacial defects through frequency-dependent C-V and conductance–frequency measurements, are required to confirm the precise interfacial origins of this response.

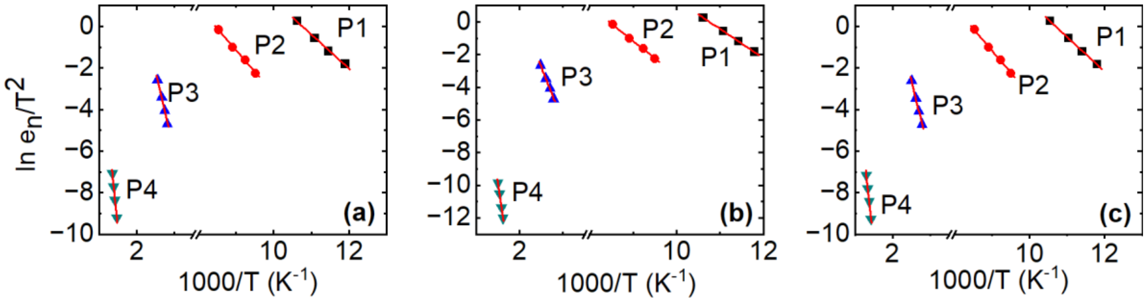

Fig 6. Arrhenius plots corresponding to the DLTS peaks shown in Fig. 5 for (a) AS050 (b) AS150 and (c) AS250 MOS detectors.

Table 2. Defect parameters obtained from DLTS measurements of MOS detectors.

Peak #	Defect Identity	Detector ID	Activation Energy (eV)	Capture Cross-section (cm^2)	Trap Concentration (cm^{-3})
P1	Ti(h)	AS050	0.14	9.3×10^{-15}	4.31×10^{11}
		AS150	0.15	3.5×10^{-14}	3.90×10^{11}
		AS250	0.14	1.02×10^{-14}	1.06×10^{11}
P2	Ti(c)	AS050	0.18	7.6×10^{-15}	1.98×10^{12}
		AS150	0.18	8.5×10^{-15}	1.92×10^{12}
		AS250	0.18	9.9×10^{-15}	4.46×10^{11}
P3	$Z_{1/2}$	AS050	0.67	6.5×10^{-15}	5.29×10^{12}
		AS150	0.57	2.1×10^{-16}	1.87×10^{12}
		AS250	0.65	1.94×10^{-15}	4.71×10^{11}
P4	$EH_{6/7}$	AS050	1.56	6.1×10^{-15}	7.72×10^{11}
		AS150	1.55	5.5×10^{-15}	1.39×10^{12}
		AS250	1.42	2.72×10^{-16}	3.79×10^{11}

5. Conclusion

This study highlights the significant potential of 4H-SiC-based metal–oxide–semiconductor (MOS) radiation detectors incorporating Y_2O_3 gate dielectrics for high-performance operation in extreme environments. By leveraging the intrinsic advantages of 4H-SiC – such as its wide bandgap, high thermal conductivity, and excellent radiation hardness – alongside the high dielectric constant, thermal stability, and favorable interface characteristics of Y_2O_3, we demonstrate enhanced electrical performance and charge transport behavior in devices with varying epitaxial layer thicknesses.

We have conducted a comprehensive investigation of Ni/Y_2O_3/4H-SiC Schottky barrier detectors fabricated on 4H-SiC epilayers of three different thicknesses: 50 µm, 150 µm, and 250 µm. The Y_2O_3 layer, deposited via pulsed laser deposition (PLD), was maintained at a thickness of 40 nm – a value previously identified as optimal for achieving favorable interface and electrical properties. Despite the inclusion of this thin dielectric layer, the devices exhibited characteristics typical of Schottky barrier diodes, owing to the minimal oxide thickness and resultant tunnelling behavior at the metal–oxide–semiconductor interface.

Electrical characterization was performed through current-voltage (I-V) and capacitance-voltage (C-V) measurements, while capacitance-based deep level transient spectroscopy (DLTS) was used to probe and quantify electrically active deep-level defects. The radiation detection capabilities of the devices were assessed by evaluating their alpha particle response and charge collection efficiency.

The variation in epilayer thickness was explored due to its known influence on charge collection efficiency, electric field distribution, and defect response. Thicker epilayers, such as the 250 µm layer, are generally expected to support increased energy deposition and broader depletion widths, which can contribute to enhanced spectral response. Interestingly, while the AS250 detector exhibited the lowest concentrations and capture cross-sections for the $Z_{1/2}$ and $EH_{6/7}$ traps, its alpha detection response did not quite match the levels observed in the AS050 and AS150 devices.

This finding is particularly intriguing in light of our previous work, which demonstrated that 250 µm-thick 4H-SiC Schottky barrier detectors – fabricated without the Y_2O_3 layer – exhibited excellent energy resolution, comparable to that of the AS050 and AS150 detectors in the present study.

The results suggest that the degraded response in the thickest detector may be influenced by interface states or localized defects at the Y_2O_3/SiC interface, although this observation may be specific to the present sample set. Future work will include further electrical characterizations such as frequency-dependent C–V and conductance–frequency measurements to quantitatively evaluate interface trap density and its correlation with detector performance. In addition, detailed surface and interface characterization, together with device-level simulations, will be carried out to better understand the origin of this behavior and to optimize the interface properties. These investigations will aim to refine the integration of high-quality dielectric layers with thick 4H-SiC epilayers to unlock the full potential of MOS-based detector architectures.

In conclusion, the results underscore the viability of incorporating 40 nm-thick Y_2O_3 gate dielectrics – deposited via PLD – into 4H-SiC-based detectors. This approach offers a promising route to fabricate robust, high-resolution radiation detectors with much higher 4H-SiC epilayers suitable for operation in harsh environments.

6. Statements and Declarations

Funding

This work was supported in part by the Center for Resilience Excellence South Carolina (CORE SC) Innovation Grant No. #10013350 (Principal Investigator (PI), Krishna C. Mandal (KCM)) and National Science Foundation (NSF), Division of Electrical, Communications and Cyber Systems (ECCS) & Division of Materials Research (DMR) Grant No. #10014332 (PI KCM).

Author Contributions

All authors contributed to the study conception and design. Material preparation, data collection and analysis were performed by Ritwik Nag, Cihan Öner, Sandeep K Chaudhuri, and Krishna C. Mandal. The first draft of the manuscript was written by Ritwik Nag and all authors commented on previous versions of the manuscript. All authors read and approved of the final manuscript.

CRediT

Conceptualization: Ritwik Nag, Cihan Öner, Sandeep K. Chaudhuri, Krishna C. Mandal; Methodology: Ritwik Nag, Cihan Öner, Sandeep K. Chaudhuri; Formal analysis and investigation: Ritwik Nag, Cihan Öner, Sandeep K. Chaudhuri, Krishna C. Mandal; Writing - original draft preparation: Ritwik Nag, Cihan Öner, Krishna C.

Mandal; Writing - review and editing: Sandeep K. Chaudhuri, Krishna C. Mandal; Funding acquisition: Krishna C. Mandal; Resources: Krishna C. Mandal; Supervision: Krishna C. Mandal.

Data availability

The datasets generated during and/or analyzed during the current study are available from the corresponding author on reasonable request.

Code availability

Not applicable.

Conflict of interest: The authors have no conflict of interest to declare that are relevant to the content of this article.

Ethical approval: Not applicable.

Consent to participate: Not applicable.

Consent for publication: Not applicable.

References:

1. S. O. Kasap, M. Z. Kabir, K. O. Ramaswami, R. E. Johanson, R. J. Curry, Charge collection efficiency in the presence of non-uniform carrier drift mobilities and lifetimes in photoconductive detectors. J. Appl. Phys. **128** (12), 1–27, (2020). doi: 10.1063/5.0017521.
2. P. Vigneshwara Raja, C. Raynaud, B. Asllani, H. Morel, D. Planson, Electrically active traps in 4H-silicon carbide (4H-SiC) PiN power diodes. J. Mater. Sci.: Mater. Electron. **34**, 34, (2023). doi: 10.1007/s10854-023-10813-z.
3. S. K. Chaudhuri, R. Nag, and K. C. Mandal, A novel Ni/Y_2O_3/4H-SiC heteroepitaxial metal–oxide–semiconductor (MOS) betavoltaic cell, J. Mater. Sci.: Mater. Electron., **34**, (6), 543, (2023). doi: 10.1007/s10854-023-09971-x.
4. P. Samanta and K. C. Mandal, Hole injection and dielectric breakdown in 6H-SiC and 4H-SiC metal-oxide-semiconductor structures during substrate electron injection via Fowler-Nordheim tunneling, Solid-State Electron.**114,** 60-68, (2015). doi: 10.1016/j.sse.2015.07.009.
5. S. K. Chaudhuri and K. C. Mandal, Radiation detection using n-type 4H-SiC epitaxial layer surface barrier detectors, in Advanced Materials for Radiation Detection, **9**. Cham, Switzerland: Springer, 183–209, (2021). doi: 10.1007/978-3-030-76461-6.
6. O. Karadavut, S. K. Chaudhuri, J. W. Kleppinger, R. Nag, and K. C. Mandal, Enhancement of radiation detection performance with reduction of $EH_{6/7}$ deep levels in n-type 4H–SiC through thermal oxidation, Appl. Phys. Lett., **121**, 012103, (2022). doi: 10.1063/5.0089236.
7. K. C. Mandal, S. K. Chaudhuri, and Frank H. Ruddy High-resolution alpha spectrometry using 4H-SiC detectors: A review of the state-of-the-art **70**, (5), 823-830, (2023). doi: 10.1109/TNS.2023.3267996
8. G. F. Knoll, Radiation Detection and Measurement, 4th ed. Hoboken, NJ, USA: Wiley, 2010, 403.
9. E. Steinbauer, P. Bauer, M. Geretschlager, G. Bortels, J. P. Biersack, and P. Burger, Energy resolution of silicon detectors: Approaching the physical limit, Nucl. Instrum. Methods Phys. Res. B, Beam Interact. Mater. At., **85**, (1–4), 642–649, (1994). doi: 10.1016/0168-583X(94)95898-X**.**
10. F. H. Ruddy, L. Ottaviani, A. Lyoussi, C. Destouches, O. Palais, and C. Reynard-Carette, Silicon carbide neutron detectors for harsh nuclear environments: A review of the state of the art, IEEE Trans. Nucl. Sci., **69,** (4), 792–803, (2022). doi: 10.1109/TNS.2022.3144125**.**
11. K. C. Mandal, P. G. Muzykov, S. K. Chaudhuri, and J. R. Terry, Low energy X-ray and γ -ray detectors fabricated on n-type 4H-SiC epitaxial layer, IEEE Trans. Nucl. Sci., **60**, (4), 2888–2893, (2013). doi: 10.1109/TNS.2013.2273673.
12. K. C. Mandal, P. G. Muzykov, and J. R. Terry, Highly sensitive X-ray detectors in the low-energy range on n-type 4H-SiC epitaxial layers, Appl. Phys. Lett., **101**, 051111, (2012). doi: 10.1063/1.4742741**.**
13. J. W. Kleppinger, S. K. Chaudhuri, O. Karadavut, and K. C. Mandal, Defect characterization and charge transport measurements in high resolution Ni/n-4H-SiC Schottky barrier radiation detectors fabricated on 250 µm epitaxial layers, J. Appl. Phys., **129**, 244501, (2021). doi: 10.1063/5.0049218.
14. R. Nag, S. K. Chaudhuri, F. H. Ruddy, and K. C. Mandal, High-resolution Cr/4H-SiC Schottky barrier radiation detector, IEEE Trans. Nucl. Sci., **72**, (4), 1644 - 1651, (2025). doi: 10.1109/TNS.2025.3547998
15. H. Fujiwara, H. Naruoka, M. Konishi, K. Hamada, T. Katsuno, T. Ishikawa, Y. Watanabe, and T. Endo, Relationship between threading dislocation and leakage current in 4H-SiC diodes, Appl. Phys. Lett., **100**, 242102, (2012). doi:10.1063/1.4718527.
16. H. J. Quah, W. F. Lim, S. C. Wimbush, Z. Lockman, and K. Y. Cheong, Electrical properties of pulsed laser deposited Y_2O_3 gate oxide on 4H–SiC, Electrochem. Solid-State Lett., **13**, (11), H396, (2010). doi: 10.1149/1.3481926.
17. D. Shi, Y. Wang, X. Wu, Z. Yang, X. Li, J. Yang, and F. Cao, Improving the barrier inhomogeneity of 4H-SiC Schottky diodes by inserting Al_2O_3 interface layer, Solid-State Electron., **180**, 107992, (2021). doi: 10.1016/j.sse.2021.107992.
18. K. C. Mandal, S. K. Chaudhuri, and F. H. Ruddy High resolution metal-oxide-4H-SiC radiation detectors: A review, IEEE Trans. Nucl. Sci.**71** (8), (2024). doi: 10.1109/TNS.2024.3422902.

19. S. K. Chaudhuri, O. Karadavut, J. W. Kleppinger, and K. C. Mandal, High-resolution radiation detection using Ni/SiO_2/n-4H-SiC vertical metal-oxide-semiconductor capacitor, J. Appl. Phys., **130**, 074501, (2021). doi: 10.1063/5.0059151.
20. Y. Jia, Y. Jia, Y. Shen, X. Sun, Z. Shi, K. Jiang, T. Wu, H. Liang, X. Cui, W. Lü, and D. Li, Improved performance of SiC radiation detector based on metal–insulator–semiconductor structures, Nucl. Instrum. Methods Phys. Res. A, Accel. Spectrom. Detect. Assoc. Equip., **997**, 165166, (2021). doi: 10.1016/j.nima.2021.165166.
21. O. Karadavut, S. K. Chaudhuri, J. W. Kleppinger, R. Nag, and K. C. Mandal, Performance-improved vertical Ni/SiO_2/4H-SiC metal– oxide–semiconductor capacitors for high-resolution radiation detection, IEEE Trans. Nucl. Sci., **69**, (8), 1965-1971, (2022). doi: 10.1109/TNS.2022.3168792.
22. P. Samanta and K. C. Mandal, Leakage current conduction, hole injection, and time-dependent dielectric breakdown of n-4H-SiC MOS capacitors during positive bias temperature stress, J. Appl. Phys., **121**, (3),034501, (2017). doi: 10.1063/ 1.4973674.
23. Z. Wang, Z. Zhang, C. Shao, J. Robertson, S. Liu, and Y. Guo, Tuning the high-k oxide (HfO_2, ZrO_2)/4H-SiC interface properties with a SiO_2 interlayer for power device applications, Appl. Surf. Sci., **527**, 146843, (2020). doi: 10.1016/j.apsusc.2020.146843.
24. R. Y. Khosa, J. T. Chen, M. Winters, K. Pálsson, R. Karhu, J. Hassan, N. Rorsman, and E. Ö. Sveinbjörnsson, Electrical characterization of high k-dielectrics for 4H-SiC MIS devices, Mater. Sci. Semicond. Process., **98**, 55–58, (2019). doi: 10.1016/j.mssp.2019.03.025.
25. T. -H. Kil, M. Noguchi, H. Watanabe, and K. Kita, Impacts of Al_2O_3/SiO_2 interface dipole layer formation on the electrical characteristics of 4H-SiC MOSFET, IEEE Electron Device Lett., **43**, (1), 92–95, (2022). doi: 10.1109/LED.2021.3125945.
26. Siddiqui, R. Y. Khosa, and M. Usman, High-k dielectrics for 4H-silicon carbide: present status and future perspectives, J. Mater. Chem. C, **9**, (15), 5055–5081, (2021). doi: 10.1039/D0TC05008C.
27. F. Zhao, O. Amnuayphol, K. Y. Cheong, Y. H. Wong, J. -Y. Jiang, and C. -F. Huang, Post deposition annealing effect on properties of Y_2O_3/Al_2O_3 stacking gate dielectric on 4H-SiC, Mater. Lett., **245**, 174–177, (2019). doi: 10.1016/J.MATLET.2019.03.009.
28. G. Apostolopoulos, G. Vellianitis, A. Dimoulas, M. Alexe, R. Scholz, M. Fanciulli, D. T. Dekadjevi, and C. Wiemer, High epitaxial quality Y_2O_3 high-k dielectric on vicinal Si(001) surfaces, Appl. Phys. Lett., **81**, (19), 3549–3551, (2002). doi: 10.1063/1.1519727.
29. V. H. Mudavakkat, V. V. Atuchin, V. N. Kruchinin, A. Kayani, and C. V. Ramana, Structure, morphology and optical properties of nanocrystalline yttrium oxide (Y_2O_3) thin films, Opt. Mater., **34**, (5), 893–900, (2012). doi: 10.1016/j.optmat.2011.11.027.
30. H. J. Quah, W. F. Lim, S. C. Wimbush, Z. Lockman, and K. Y. Cheong, Electrical properties of pulsed laser deposited Y_2O_3 gate oxide on 4H-SiC, Electrochem. Solid-State Lett., **13**, (11), H396, (2010). doi: https://doi.org/10.1149/1.3481926.
31. S. K. Chaudhuri, O. Karadavut, J. W. Kleppinger, R. Nag, G. Yang, D. Lee, and K. C. Mandal, Enhanced hole transport in Ni/Y_2O_3/n-4H-SiC MOS for self-biased radiation detection, IEEE Electron Device Lett., **43**, (9), 1416–1419, (2022). doi: 10.1109/LED.2022.3188543.
32. K. C. Mandal, S. K. Chaudhuri, and F. H. Ruddy, High resolution metal-oxide-4H-SiC detectors with various high-k dielectric oxide layers, *2023 IEEE Nuclear Science Symposium, Medical Imaging Conference and International Symposium on Room-Temperature Semiconductor Detectors (NSS MIC RTSD)*, Vancouver, BC, Canada, 2023, pp. 1-2, doi: 10.1109/NSSMICRTSD49126.2023.10337975.
33. O. Karadavut, J. W. Kleppinger, S. K. Chaudhuri, and Krishna C. Mandal, Effect of enhanced hole transport on the performance of Ni/Y_2O_3/n-4H-SiC epilayer radiation detectors, IEEE Trans. Nucl. Sci., **70**, (9), 2264-2272, (2023). doi: 10.1109/TNS.2023.3306276.
34. J. W. Kleppinger, S. K. Chaudhuri, O. Karadavut, R. Nag, and K. C. Mandal, Influence of carrier trapping on radiation detection properties in CVD grown 4H-SiC epitaxial layers with varying thickness up to 250 μm, J. Cryst. Growth, **583**, 126532, (2022). doi: 10.1016/j.jcrysgro.2022.126532.
35. W. Kern, The evolution of silicon wafer cleaning technology, J. Electrochem. Soc., **137**, (6), 1887–1892, (1990). doi: 10.1149/1.2086825.

36. D. H. Lowndes, D. B. Geohegan, A. A. Puretzky, D. P. Norton, and C. M. Rouleau, Synthesis of novel thin-film materials by pulsed laser deposition, Science, **273**, (5277), 898–903, (1996). doi: 10.1126/science.273.5277.898.
37. S. K. Chaudhuri, K. J. Zavalla, and K. C. Mandal, Experimental determination of electron-hole pair creation energy in 4H-SiC epitaxial layer: An absolute calibration approach, Appl. Phys. Lett., **102**, 031109, (2013). doi: 10.1063/1.4776703.
38. S. M. Sze and K. K. Ng, Physics of Semiconductor Devices, John Wiley & Sons, New York, (2007).
39. R. T. Tung, J. P. Sullivan, F. Schrey, On the inhomogeneity of Schottky barriers, Appl. Phys. Lett., **14**, (3), 266–280, (1992). doi: 10.1016/0921-5107(92)90309-W.
40. M. A. Mannan, S. K. Chaudhuri, K. V. Nguyen, and K. C. Mandal, Effect of $Z_{1/2}$, EH_5, and Ci1 deep defects on the performance of n-type 4H-SiC epitaxial layers Schottky detectors: Alpha spectroscopy and deep level transient spectroscopy studies, J. Appl. Phys., **115**, (22), 224504, (2014). doi: 10.1063/1.4883317.
41. K. C. Mandal, S. K. Chaudhuri, K. V. Nguyen, and M. A. Mannan, Correlation of deep levels with detector performance in 4H-SiC epitaxial Schottky barrier alpha detectors, IEEE Trans. Nucl. Sci., **61**, (4), 2338–2344, (2014). doi: 10.1109/TNS.2014.2335736.
42. M. B. H. Breese, A theory of ion beam induced charge collection, J. Appl. Phys., **74**, (6), 3789–3799, (1993). doi: 10.1063/1.354471.
43. J. F. Ziegler, M. D. Ziegler, and J. P. Biersack, SRIM—The stopping and range of ions in matter, Nucl. Instrum. Methods Phys. Res. B, Beam Interact. Mater. At., **268**, (11–12), 1818–1823, (2010). doi: 10.1016/j.nimb.2010.02.091.
44. D. V. Lang, Deep-level transient spectroscopy: A new method to characterize traps in semiconductors, J. Appl. Phys., **45**, (7), 3023–3032, (1974). doi: 10.1063/1.1663719.
45. L. Storasta, J. P. Bergman, E. Janzén, A. Henry, and J. Lu, Deep levels created by low energy electron irradiation in 4H-SiC, J. Appl. Phys., **96**, (9), 4909–4915, (2004). doi: 10.1063/1.1778819.
46. L. Storasta, H. Tsuchida, T. Miyazawa, and T. Ohshima, Enhanced annealing of the $Z_{1/2}$ defect in 4H–SiC epilayers, J. Appl. Phys., **103**, 031109, (2008). doi: 10.1063/1.2829776.
47. K. C. Mandal, R. M. Krishna, P. G. Muzykov, S. Das, and T. S. Sudarshan, Characterization of semi-insulating 4H silicon carbide for radiation detectors, IEEE Trans. Nucl. Sci., **58**, (4), 1992-1999, (2011). doi: 10.1109/TNS.2011.2152857.
48. L. Storasta, J. P. Bergman, E. Janzén, A. Henry and J. Lu, Deep levels created by low energy electron irradiation in 4H-SiC, J. Appl. Phys., **96**, (9), 4909–4915, (2004). doi: 10.1063/1.1778819.
49. S. A. Reshanov, G. Pensl, K. Danno, T. Kimoto, S. Hishiki, T. Ohshima, H. Itoh, F. Yan, R. P. Devaty, and W. J. Choyke, Effect of the Schottky barrier height on the detection of midgap levels in 4H-SiC by deep level transient spectroscopy, J. Appl. Phys., **102**, 113702, (2007). doi: 10.1063/1.2818050.
50. M. A. Mannan, K. V. Nguyen, R. O. Pak, C. Oner, and K. C. Mandal, Deep levels in n-type 4H-silicon carbide epitaxial layers investigated by deep-level transient spectroscopy and isochronal annealing studies, IEEE Trans. Nucl. Sci., **63**, (2), 1083–1090, (2016). doi: 10.1109/TNS.2016.2535212.
51. P. G. Muzykov, R. M. Krishna, and K. C. Mandal, Characterization of deep levels in n-type and semi-insulating 4H-SiC epitaxial layers by thermally stimulated current spectroscopy, J. Appl. Phys., **111**, 014910, (2012). doi: 10.1063/1.3675513.
52. J. W. Kleppinger, S. K. Chaudhuri, O. Karadavut, R. Nag, D. L. P. Watson, D. S. McGregor, and K. C. Mandal, Deep-level transient spectroscopy and radiation detection performance studies on neutron irradiated 250-µm-thick 4H-SiC epitaxial layers, IEEE Trans. Nucl. Sci.**69**, (8), 1972-1978, (2022). doi: 10.1109/TNS.2022.3168789.